JACS
JOURNAL OF THE AMERICAN CHEMICAL SOCIETY
pubs.acs.org/JACS
Article

Agglomeration Drives the Reversed Fractionation of Aqueous Carbonate and Bicarbonate at the Air−Water Interface

Shane W. Devlin, Sasawat Jamnuch, Qiang Xu, Amanda A. Chen, Jin Qian,* Tod A. Pascal,* and Richard J. Saykally*

Cite This: https://doi.org/10.1021/jacs.3c05093
Read Online
ACCESS | Metrics & More | Article Recommendations | Supporting Information

ABSTRACT: In the course of our investigations of the adsorption of ions to the air−water interface, we previously reported the surprising result that doubly charged carbonate anions exhibit a stronger surface affinity than singly charged bicarbonate anions. In contrast to monovalent, weakly hydrated anions, which generally show enhanced concentrations in the interfacial region, multivalent (and strongly hydrated) anions are expected to show a much weaker surface propensity. In the present work, we use resonantly enhanced deep-UV second-harmonic generation spectroscopy to measure the Gibbs free energy of adsorption of both carbonate (CO_3^{2-}) and bicarbonate (HCO_3^-) anions to the air−water interface. Contrasting the predictions of classical electrostatic theory and in support of our previous findings from X-ray photoelectron spectroscopy, we find that carbonate anions do indeed exhibit much stronger surface affinity than do the bicarbonate anions. Extensive computer simulations reveal that strong ion pairing of CO_3^{2-} with the Na^+ countercation in the interfacial region results in the formation of near-neutral agglomerate clusters, consistent with a theory of interfacial ion adsorption based on hydration free energy and capillary waves. Simulated X-ray photoelectron spectra predict a 1 eV shift in the carbonate spectra compared to that of bicarbonate, further confirming our experiments. These findings not only advance our fundamental understanding of ion adsorption chemistry but also impact important practical processes such as ocean acidification, sea-spray aerosol chemistry, and mammalian respiration physiology.

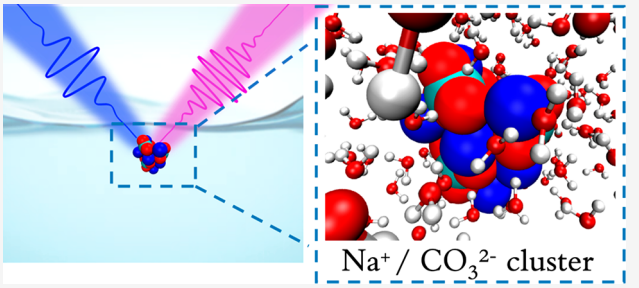

INTRODUCTION

Chemistry occurring at aqueous interfaces governs many important phenomena, e.g., reactions in atmospheric aerosols[1,2] and the uptake of gases at the ocean surface,[3] as well as myriad biological processes. Reactions occurring at such an interface are often quite distinct from the same processes occurring in the corresponding bulk. Accordingly, much attention has addressed interfacial chemistry to understand the physical origins engendering these differences, with factors such as dielectric constants,[4−6] unique hydrogen-bonding networks,[7,8] electric double-layer formation,[9−11] and electric fields,[12] being invoked to rationalize the observed behavior.

The discovery that anions with weak hydration enthalpies can have strongly enhanced concentrations in the interfacial region is a relatively new phenomenon,[13] which initially contradicted classical electrostatic theory and the interpretation of many "surface-sensitive" experiments, e.g., the change in surface tension of water upon addition of salt.[14] Several inconsistencies have since been reconciled, and our understanding is now much more complete, with even the detailed mechanism of adsorption for weakly hydrated, monovalent anions to water−hydrophobe interfaces being quite well established.[15−17] However, the picture remains unclear for strongly hydrated, polyatomic ions such as CO_3^{2-} and SO_4^{2-}, which generally experience stronger image charge repulsion from the water−hydrophobe boundary. Given the importance of many strongly hydrated, polyoxy anions (e.g., CO_3^{2-}, SO_4^{2-}, PO_4^{3-}, NO_3^-, XO_3^-, X = Cl, Br, I, and their respective acids) in atmospheric, environmental, and biological systems, further investigation of their behavior at the air−water interface is clearly warranted.

Our focus herein is on the centrally important carbonate system, which has been studied extensively, dating back to solubility experiments conducted over 100 years ago.[18] The hydration structure and dynamics of carbonate species have been characterized with a number of different methods, including MD simulation,[19,20] quantum calculations,[21−23] and X-ray spectroscopy.[24−28] Similarly, surface-sensitive nonlinear spectroscopies have been used to study the behavior of these important anions. An early vibrational sum-frequency generation (vSFG) study by Tarbuck and Richmond reported that

Received: May 16, 2023
Published: September 29, 2023

Na_2CO_3 perturbs the air−water interface more than $NaHCO_3$ does; however, the authors did not comment on the relative surface affinities of the two anions.[3] Allen et al. conducted phase-sensitive measurements and found an increase in H-down oriented interfacial waters in the presence of carbonate and concluded that the sodium countercation resides closer to the air−water interface than does the anion and that bicarbonate resides closer to the surface than carbonate.[29] MD simulations purportedly supported these findings.[30,31] It has also been reported recently that the carbonate system does not form a well-ordered electric double layer.[32] We note that these vSFG measurements monitor solute-induced changes in the OH spectrum of water and are, therefore, *indirect* measures of the interfacial ion population. Moreover, there is still some debate in the literature regarding the interpretation of these measurements.[33−35]

We recently reported the reversed fractionation of carbonate and bicarbonate anions at the air−water interface using ambient pressure X-ray photoelectron spectroscopy (AP-XPS). These were the first direct experimental measurements of the carbonate species, and we found higher concentrations of doubly charged carbonate ions than singly charged bicarbonate in the near-interfacial region, contrasting previous nominally surface-sensitive measurements. Without detailed theory to interpret this surprising behavior and given that AP-XPS is not rigorously a surface-sensitive technique, we herein revisit the subject of the interfacial adsorption behavior of the carbonate system. In particular, we aim to clarify the discrepancies that exist in the literature regarding the relative surface affinity of the carbonate and bicarbonate anions at the air−water interface and to propose a molecular-level picture for their observed surface behavior.

In this work, we employ resonantly enhanced deep-UV second-harmonic generation (DUV-SHG) spectroscopy to *directly* probe the carbonate and bicarbonate anions at the air−water interface with much higher surface specificity than the AP-XPS experiment. We find, contrary to classical electrostatic theory and in agreement with our previous AP-XPS measurements, that the doubly charged carbonate anion does indeed exhibit a stronger preference for the air−water interface than does the singly charged bicarbonate anion and quantify this through the determination of the respective Gibbs free energies of adsorption. To obtain more detailed mechanistic insights into these phenomena, we employ accelerated molecular dynamics (MD) simulations, using a physics-based, polarizable force field to map the two-dimensional free energy surface of carbonate agglomeration and propensity for adsorption at the interface. These simulations reveal enhanced speciation, and a deep potential minima, of the carbonate species near the interface. Lastly, we establish a direct connection with our previous experiments by simulating the XPS binding energies of the carbonate, bicarbonate, and carbonic acid species, showing that these previous experiments were indeed interface sensitive (to within 2 nm of the water surface).

METHODS

SHG and the Langmuir Adsorption Model as Direct Probes of the Interfacial Structure. To directly probe the carbonate and bicarbonate anions at the air−water interface, we use resonantly enhanced DUV-SHG spectroscopy. SHG is a second-order nonlinear spectroscopic technique wherein two photons at frequency ω combine to form one photon at frequency 2ω. Symmetry requirements under the electric dipole approximation dictate that a SH photon is only generated in a noncentrosymmetric environment (i.e., an interface) and from a noncentrosymmetric molecule, rendering SHG a highly surface-specific technique.[36] The SH intensity is governed by the equation

$$I_{SH} \propto |\chi^{(2)}|^2 I_\omega^2 \tag{1}$$

where $\chi^{(2)}$ is the second-order susceptibility and I_{SH} and I_ω are the intensities of the fundamental and SH beams, respectively. Both the anions and water have their respective susceptibility tensors and contribute to the overall signal:

$$\frac{I_{SH}}{I_\omega^2} \propto |N_{water} \times \beta_{water}^{eff} + N_{anion} \times \beta_{anion}^{eff}|^2 \tag{2}$$

The molecular responses for the anion and water are complex and contain both a real (nonresonant) and an imaginary (resonant) component. In the UV, the response from water is purely real. Therefore, under the two-photon-resonant conditions employed here, the resonant term from the anion should dominate the overall measured SH intensity.

In the low solute concentration regime and/or under nonresonant conditions, the signal from water and the solute need to be considered more equally, which will be discussed in more detail later. We can express the resonant term for the anion as

$$\chi_{anion}^{(2)} \propto N_{anion} \langle \beta_{anion} \rangle \tag{3}$$

here β_{anion} is the orientationally averaged hyperpolarizability and N represents the number density of the anion at the interface. Equation 3 emphasizes that changes in the surface population, as well as the orientation of the resonant species, will change the measured SH signal.

The SH signal depends on the relative concentration of the adsorbing solute; thus, we can apply a simple Langmuir model to fit our experimental data. The use of a Langmuir model for SHG is well established,[37] and only the important features are highlighted here (for a more thorough derivation, we refer the reader to the Supporting Information). We parametrize the second-order susceptibility as

$$|\chi^{(2)}|^2 \propto |A + N_s(B + iC)|^2 \tag{4}$$

where A represents the nonresonant response from water, N_s is the relative number density of the adsorbed anion, and B and C are the nonresonant and resonant susceptibilities of the anion, respectively. N_s is determined from a kinetic description of surface exchange and related to the bulk anion concentration, X_{anion^-} and Gibbs free energy of adsorption, ΔG:

$$\begin{aligned} \frac{I_{2\omega}}{I_\omega^2} &\propto |\chi^{(2)}|^2 \\ &\propto \left(A + B \frac{X_{anion}}{(1 - X_{anion}) e^{\Delta G/RT} + X_{anion}} \right)^2 \\ &\quad + \left(C \frac{X_{anion}}{(1 - X_{anion}) e^{\Delta G/RT} + X_{anion}} \right)^2 \end{aligned} \tag{5}$$

Thus, by measuring the second-harmonic (SH) intensity as a function of the anion concentration, the Gibbs free energy of adsorption can be determined.

Energy Landscapes of Interfacial Agglomeration Energy from Accelerated MD Simulations. Early simulations of solvated sodium carbonates either employed static charges[38] or modeled polarization by means of Drude oscillators.[38−43] However, it has been demonstrated recently[44] that more accurate considerations of the subtle polarization physics are needed to faithfully reproduce the experiments, namely, simultaneously describing the crystalline solid and solvated carbonate phases.[45] These results largely motivated our choice of interaction potentials in this study.

https://doi.org/10.1021/jacs.3c05093
J. Am. Chem. Soc. XXXX, XXX, XXX−XXX

The carbonate and bicarbonate interfacial affinity were probed using atomistic MD simulations, carried out using the large-scale atomic/molecular massively parallel simulator (LAMMPS),[46] with the various molecules described by the AMOEBA polarizable force field[47] for carbonates.[44,45,48] Four separate systems, comprising sodium carbonate (Na_2CO_3), sodium bicarbonate ($NaHCO_3$), carbonic acid (H_2CO_3), and carbon dioxide (CO_2), as detailed in Table S2, were constructed, using in-house Python scripts. The number of water molecules was adjusted to approximately match the experimental 0.1 M concentrations. We validated our approach by calculating hydration free energies (Table S3) in good agreement with experiment. Additionally, application of the force field to natrite, thermonatrite, sodium hydrogen carbonate, and carbon dioxide resulted in calculated lattice constants within 2.5% of experiments (Table S4).

Each carbonate system was first equilibrated at 298 K in a bulk (3D) geometry, while a separate set of slab (2D) simulations was performed using the equilibrated coordinates and velocities from the bulk simulations as input. We determined the potential energy surface for agglomeration and the propensity for interfacial adsorption by means of multiple-walker, well-tempered, metadynamics simulations (MW-wt-MetaD),[49−52] using the Colvars[53] facility. MW-wt-MetaD biases were constructed as follows: Gaussian functions were deposited every 1.0 ps with an initial height of $277T \times 5.0$ kJ/mol. The bias factor $[\gamma = (T + \Delta T)/T]$ was set to 10. The Gaussian widths were 0.02 for the coordination number about a central carbonate molecule (monitoring the carbon−carbon distances) and 0.2 Å for the Z-displacement of the selected carbonate molecule from the center of mass of the water slab, respectively. To facilitate exploration of the entire 2D potential energy surface in a computationally tractable time, 35 walkers were used, with each individual simulation propagated for at least 30 ns in the case of Na_2CO_3 (representing >1 ms of simulation time). Further details of the specific force field parameters, our structural and thermodynamic analysis, and various MD simulation procedures are presented in the Supporting Information.

Electronic Structure of the Carbonate−Water Interface from Simulated XPS. We performed separate sets of MD simulations on a smaller system to generate snapshots for the electronic structure calculations. Each set of simulations had representative structures of the targeted carbon-containing chemical species at the air−water interface and in the bulk. Due to the enormous computational cost, we employed the ARES electronic structure package[54] to simulate XPS binding energies of C K-edge excitation in carbonate aqueous solution.

RESULTS/DISCUSSION

Second-Harmonic Generation Spectroscopy. Figure 1a shows the bulk absorption spectra of Na_2CO_3 and $NaHCO_3$ in water at 293 K, with both anions exhibiting molecular $\pi\pi^*$ transitions in the deep UV. The geometries of the carbonate and bicarbonate anions in solution have been well characterized; quantum chemical calculations[21] and neutron diffraction[55] showed that the normally planar CO_3^{2-} anion exhibits broken symmetry in aqueous solution ($D_{3h} \rightarrow C_{3v}$) due to interactions with the solvent. Raman spectroscopy studies in solution have also concluded that the first-shell solvation environment is indeed itself asymmetric.[56] These properties of the carbonate and bicarbonate anions allow us to directly probe their relative concentrations in the interfacial region. A cartoon depiction of the experimental design is shown in Figure 1b.

Figure 2a shows the normalized (relative to pure water) SH response of the carbonate anion at the air−water interface for 0−0.036 mole fraction (0−2.0 M) solutions of sodium carbonate. The intensities are measured in two polarization combinations (*s*-in, *p*-out and *p*-in, *p*-out), with both polarizations giving a fairly weak second-order response, ca.

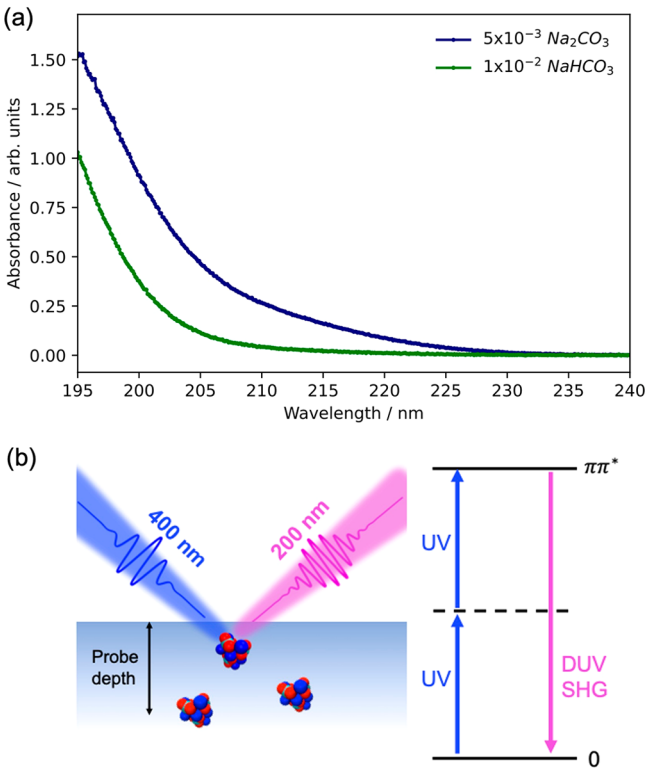

Figure 1. (a) Linear absorption spectra for 5×10^{-3} M Na_2CO_3 (blue line) and 1×10^{-2} M $NaHCO_3$ (green line) measured at 293 K. (b) Schematic of the experimental design showing the generation of a second-harmonic photon from a carbonate cluster residing near the liquid water surface. The energy-level diagram highlights the two-photon resonant enhancement from the molecular $\pi\pi^*$ transition of the carbonate and bicarbonate anions.

twice the response of pure water at a concentration of 2.0 M bulk concentration; this is likely due to the small extinction coefficient at 200 nm for carbonate when compared to other surface-active anions such as SCN^-, which exhibits a much stronger SH response.[57] In the low-concentration region from 0 to 0.0045 mole fraction (0−0.175 M), the measured SH response is slightly below or equal to that of pure water, indicating no appreciable amount of carbonate in the probe depth of SHG, as well as minimal reorientation of interfacial water molecules.

Electrolyte solutions with normalized SHG values below the response of pure water have been observed previously in the low-concentration limit, and the mechanism for this response is still debated in the literature. Explanations such as destructive interference between the resonant signal from the electrolyte and the nonresonant signal from water have been implicated;[58,59] however, more recent studies seem to point toward long-range correlations extending from bulk water, induced by the electrolyte, as the cause of this behavior.[60,61] This phenomenon is most relevant for the discussion of the Jones−Ray effect in sub-molar concentrations and is not a focus of the present work.

Between 0.0045 and 0.018 mole fraction (0.175 and 1.0 M), the SH response begins to increase linearly with anion concentration, owing to resonant enhancement of carbonate as it accumulates in the interface, as well as alignment of interfacial water from the electric field of the electrolyte. The latter contribution effectively increases the hyperpolarizability of water (see eq 3) and is akin to a "thickening" of the

https://doi.org/10.1021/jacs.3c05093
J. Am. Chem. Soc. XXXX, XXX, XXX−XXX

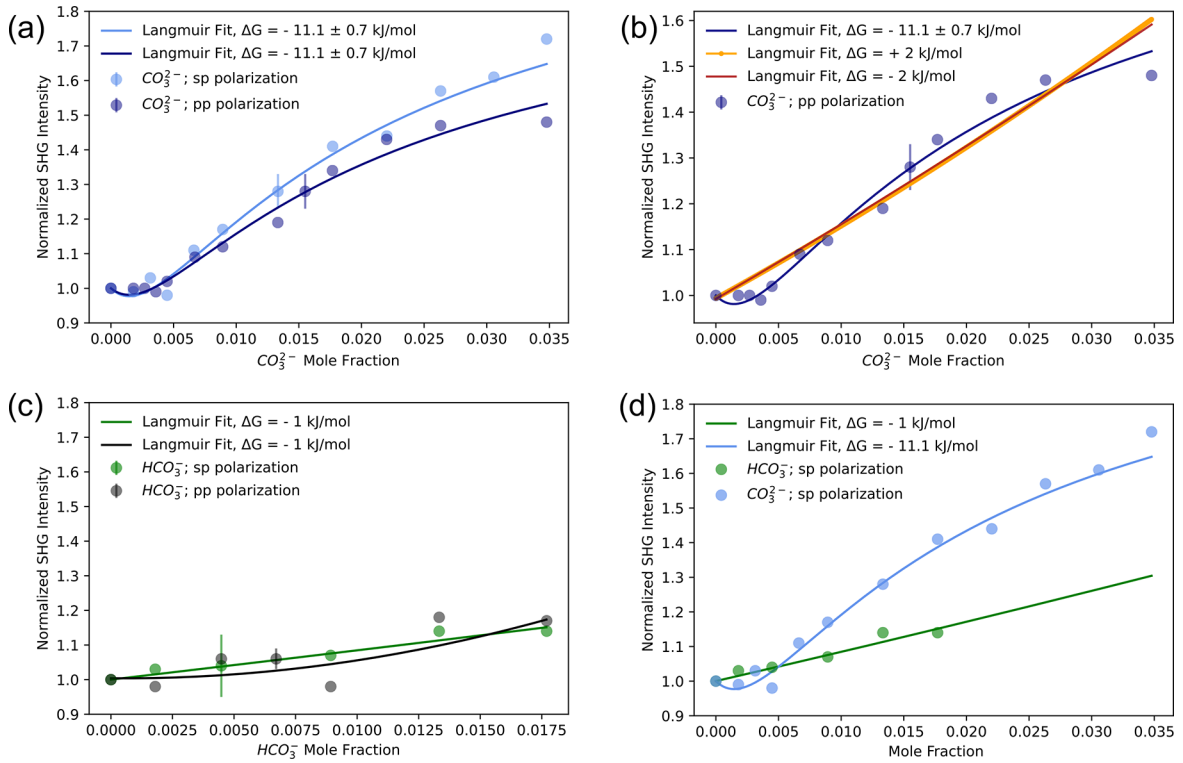

Figure 2. (a) Normalized SHG intensities for the carbonate anion at the air−water interface, measured at a SH wavelength of 200 nm for *s*-in, *p*-out (light blue circles) and *p*-in, *p*-out (dark blue circles). For clarity, only one representative error bar for each data set is shown, which corresponds to one standard deviation. Each data set is fit to a Langmuir adsorption model, yielding Gibb's free energies of adsorption of −11.1 ± 0.7 kJ/mol. (b) Langmuir adsorption model shown for three different adsorption regimes for the carbonate anion: strong adsorption (dark blue), weak adsorption (red), and repulsion (orange). (c) Normalized SHG intensities of the bicarbonate anion at the air−water interface, measured at an SH wavelength of 200 nm for *s*-in, *p*-out (green circles) and *p*-in, *p*-out (black circles). A Langmuir fit with the Gibb's free energy constrained to −1 kJ/mol is shown for each data set. This value represents a minimum threshold for the Gibb's free energy. (d) SHG intensities for carbonate and bicarbonate. Extrapolation of the Gibbs free energy for the bicarbonate fit to concentrations of 2 M reveals an SH response significantly weaker than that for carbonate.

interface, as the probe depth of SHG increases.[62] Above 0.018 mole fraction (1.0−2.0 M), the SH response becomes asymptotic, as the surface becomes "saturated" and cannot accommodate any additional carbonate molecules. The concentration range used in these experiments is limited by the solubility of sodium carbonate, which at room temperature is ∼2 M. The Langmuir adsorption model, as employed herein, gives an unconstrained, best fit to the data with a Gibbs free energy of adsorption of −11.1 ± 0.7 kJ/mol for both *p*-in, *p*-out and *s*-in, *p*-out polarizations, with the uncertainty being one standard deviation.

Given that the *sp* and *pp*-polarization combinations yield similar SH intensities, it can be assumed that there is no strong orientational preference for the carbonate anion in the interfacial region. This is expected in the context of the agglomeration between CO_3^{2-} and Na^+ (discussed in the next section), which forms neutral clusters. Without a strong charge or dipole, there is no energetic preference for a given orientation at the surface.

In Figure 2b, right panel, we compare the best fit of the Langmuir model for the carbonate anion (−11.1 ± 0.7 kJ/mol) with the output of the Langmuir model in the weak adsorption regime (−2 kJ/mol, orange line) and the repulsive regime (+2 kJ/mol, blue line). In order to obtain these fits corresponding to weak and repulsive adsorption, the Gibbs free energy was constrained to these values, and the fitting parameters *A*, *B*, and *C* were simultaneously solved for. Both the −2 and +2 kJ/mol fits increase linearly with increasing bulk anion concentration and clearly do not adequately represent the observed curvature in the experimental data. In the weak and repulsive adsorption regime, the nonresonant parameter *B* increases, and the resonant parameter, *C*, becomes very small or even negative (see Table S1). Under the experimental conditions employed here, wherein the SH wavelength is resonant with the anion, these fitting parameters are unphysical, implying that the Langmuir model does not produce a representative fit to the data.

Figure 2c shows the normalized SH response of the bicarbonate anion from 0 to 0.0175 mole fraction (0−1.0 M) solutions of sodium bicarbonate. With both s- and p-input polarizations, there is a weak, linear increase in the SH signal with increasing bulk anion concentration. This behavior, as mentioned above, is ascribed to a thickening of the interfacial layer via alignment of surface waters and has been observed before in nonresonant studies of anions that are known to be repelled from the interface, e.g., the fluoride anion, F^-.[62]

A fit of the bicarbonate data to the Langmuir model does not converge, and therefore, the Gibbs free energy cannot be determined from an unconstrained fit. Instead, in Figure 2c, constrained fits with Gibbs free energies of −1 kJ/mol are shown for both data sets. This value of the Gibbs free energy corresponds to a weak adsorption event. More negative values of the Gibbs free energy (i.e., stronger adsorption) induce curvature in the fit that is not present in the experimental data;

https://doi.org/10.1021/jacs.3c05093
J. Am. Chem. Soc. XXXX, XXX, XXX−XXX

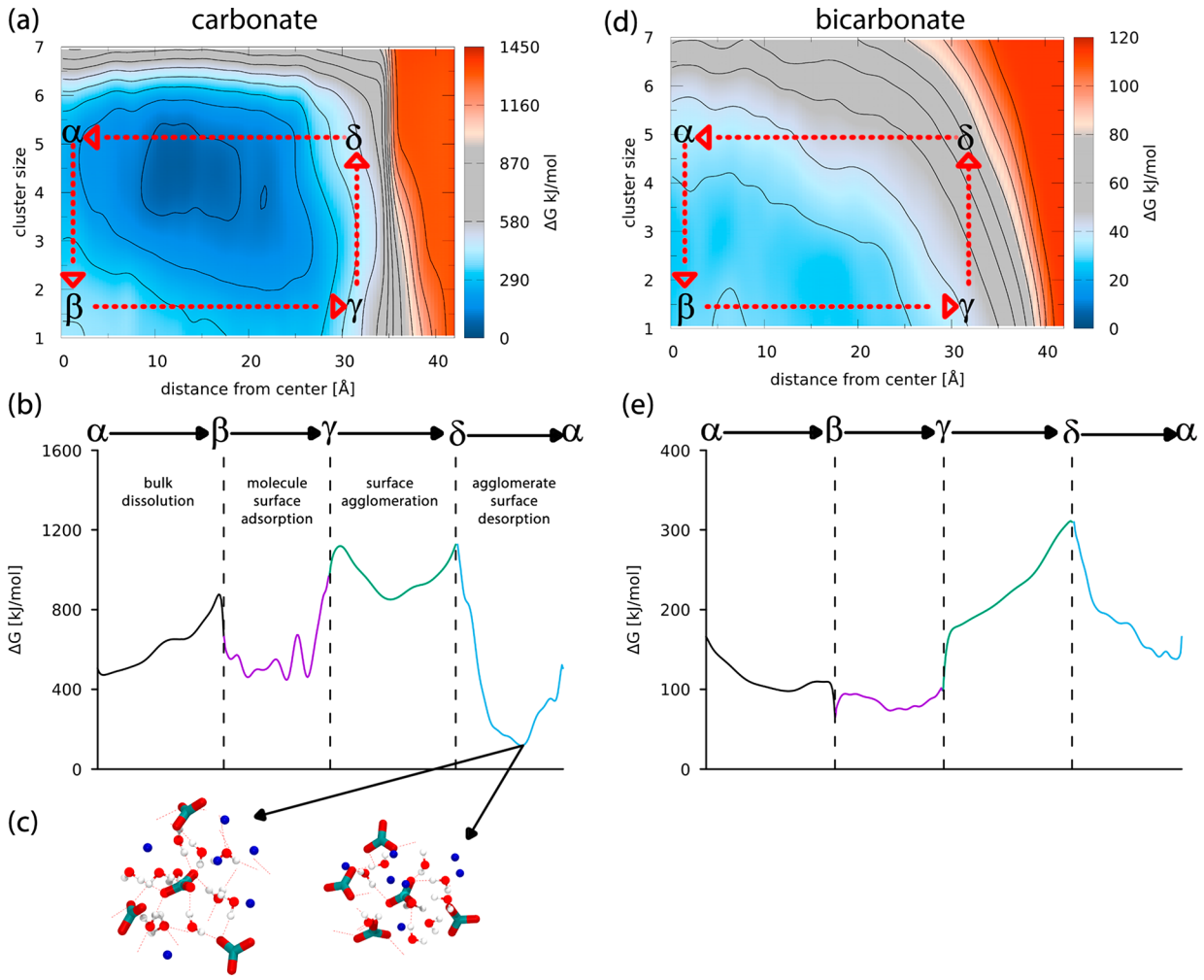

Figure 3. Accelerated MD simulations of carbonate agglomeration and surface adsorption. (a) 2D metadynamics potential energy surface (PES) of a 0.2 M Na_2CO_3 solution considering the carbonate coordination number (i.e., cluster size) and distance from the center of the slab. The simulation data are processed through a low-pass filter for presentation purposes. The water surface extends up to 3.2 nm. Specific points are labeled α, β, γ, and δ representing straight pathways (red dashed lines) for describing the thermodynamics. (b) Pathways for carbonate agglomeration/dissolution and surface adsorption/desorption. (c) Representative snapshots of the carbonate four- and five-molecule clusters. (d) $NaHCO_3$ 2D PES. (e) $NaHCO_3$ free energy pathways.

therefore, an upper limit of −1 kJ/mol is established. Less negative and positive values of the Gibb's free energy produce results that are identical to those of the −1 kJ/mol fit, viz., a shallow linear increase with increasing anion concentration. Therefore, while we cannot quantitatively determine the Gibbs free energy of adsorption for the bicarbonate anion, we can establish a range of values, with an upper limit of −1 kJ/mol and less favorable values of adsorption being more likely.

Our DUV-SHG measurements indicate that the carbonate anion has a much stronger surface affinity for the air−water interface than does the bicarbonate anion, as shown in Figure 2d. On the basis of hydration free energy ($\Delta G_{hyd}(CO_3^{2-})$ = −1315 kJ/mol and $\Delta G_{hyd}(HCO_3^-)$ = −335 kJ/mol),[63] this behavior is indeed puzzling. It has been shown by both experiment and theory that weakly hydrated anions tend to be surface active, whereas strongly hydrated anions tend to be surface repelled, roughly following the Hofmeister series.[64,65] For example, anions that have been shown to have enhanced concentrations in the interfacial region, e.g., I^- and SCN^-, have hydration free energies of ∼−280 kJ/mol. The surface adsorption of such a strongly hydrated anion as carbonate indeed seems unlikely, and we turn to computer simulations of these systems to help interpret these surprising experimental results.

Insights from Atomistic Molecular Dynamics Simulations. We performed equilibrium MD simulations of sodium carbonate solutions in a slab, 2D geometry, and concentrations ranging from 0.1 to 1 M and found that the distribution and coordination of carbonate anions were dependent on the starting configurations (Figure S1). We also found that annealing the system to 600 K (while applying constraints to prevent excessive evaporation and thus maintain slab stability) removed much of the starting configuration effect, resulting in well-dispersed, isolated Na_2CO_3 species with no significant surface activity. This is in line with previous MD simulations using unoptimized, polarizable force fields, initiated from randomly placed ions.[30,31] Nevertheless, our initial observations suggest the presence of metastable states in the carbonate free energy surface (FES), with barriers that may be significantly larger than kT and would therefore not be overcome on the nanosecond time scale of typical equilibrium MD simulations. Thus, we explored the carbonate propensity

https://doi.org/10.1021/jacs.3c05093
J. Am. Chem. Soc. XXXX, XXX, XXX−XXX

for agglomeration and surface activity by means of accelerated metadynamics MD simulations, probing the carbonate−carbonate coordination number (i.e., cluster size) and distance from the air/water interface, respectively.

Metadynamics simulations were performed on 0.1 M carbonate and bicarbonate solutions, considering agglomerate clusters up to size 7, residing 0−4 nm from the water surface. Figure 3a shows that the resulting 2D FES for the carbonate anion has a deep minimum for clusters with four or five molecules, 1−1.5 nm from the water surface. We considered the following cycle for describing the thermodynamics: (1) dissolution of the agglomerate clusters into isolated molecules in the bulk ($\alpha \rightarrow \beta$), (2) surface adsorption of the isolated molecules ($\beta \rightarrow \gamma$), (3) surface agglomeration ($\gamma \rightarrow \delta$), and (4) surface desorption of the agglomerate ($\delta \rightarrow \alpha$). As shown in Figure 3b, the isolated carbonate anions are repelled from the interface and there exists a considerably larger barrier for surface agglomeration than in the bulk. Moreover, the bulk isolated anion is metastable compared to the near-surface agglomerate. Thus, the lowest energy pathway for agglomeration follows the $\beta \rightarrow \alpha \rightarrow \gamma$ pathway. Representative molecular snapshots of these agglomerates are shown in Figure 3c.

The potential energy surface (PES) of the carbonate anion stands in contrast to that of bicarbonate, where we find that the thermodynamically stable state is that of an isolated anion, lying closer to the bulk (3−3.5 nm away from the surface) (Figure 3d). There exists some thermodynamic driving force for agglomeration to form small $(NaHCO_3)_2$ and $(NaHCO_3)_3$ clusters, although the barriers are relatively large (∼20 kJ/mol) and therefore may not be thermally accessible. Larger agglomerate clusters, such as those observed for the carbonate anion, are greatly disfavored, either in the bulk or near the interface. The PES for carbonic acid and CO_2 are presented in Figures S2 and S3. In the case of the former, we find that the isolated H_2CO_3 molecules are greatly thermodynamically stable either in the bulk or near the interface, whereas CO_2, with an unfavorable ∼+4 kJ/mol hydration energy, is thermodynamically stable near the water surface or in the vapor phase.

Given the large difference in hydration free energy for these anions, one would expect the carbonate−water coordination number to be significantly higher than that for bicarbonate. Indeed, this has been observed in the radial distribution functions for carbonate and bicarbonate anions from MD simulation, with no countercations present in the solutions.[20] The observed difference results from increased electron density on the oxygens of carbonate, coupled with a higher prevalence of sodium cations, which compete with water for interaction in the solvation environment. In the case of bicarbonate, which has a reduced electron density and half the number of sodium cations, interaction with the water is more likely. This behavior manifests in the formation of a weakly solvated agglomerate for CO_3^{2-}. The $Na^+|CO_3^{2-}$ agglomerate, which is relatively neutral and weakly hydrated, leads to a higher propensity for the interface relative to the charged HCO_3^-.

That the carbonate agglomerate shows higher surface propensity than its nonclustered, charged counterpart, as well as bicarbonate, agrees with current descriptions of ion adsorption. Saykally and Geissler have shown that there is an enthalpic benefit for weakly solvated ions to partition to the air−water interface,[16] viz., the shedding of one or two solvating waters, which can then form stronger hydrogen bonds as part of the bulk water network. How capillary waves are influenced in the presence of this large agglomerate is still an open question and could have important consequences for processes, such as gas adsorption onto the liquid surface and evaporation kinetics.

Confirmation of AP-XPS Measurements. As mentioned earlier, Lam et al. used AP-XPS to directly probe the carbon K-edge of the carbonate and bicarbonate anions at the air−water interface and measure their relative concentrations (Figure 4b).[25] By tuning the input photon energy, they exploited different attenuation lengths of the emitted photoelectron and were able to achieve depth profiling as shallow as ∼2 nm. Their findings agreed with those of the present study, viz., that CO_3^{2-} is more prevalent in the interface than HCO_3^-. However, as was noted above, AP-XPS probes deeper into the interface than do second-order spectroscopies. Even with a minimum electron attenuation length of 2 nm, there is significant signal measured from probe depths as deep as 5 nm.

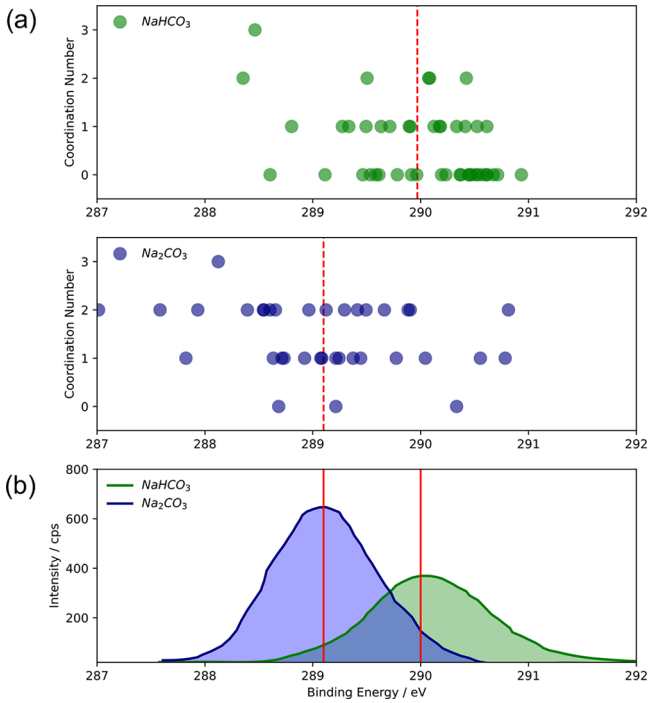

Figure 4. (a) Simulated XPS binding energies for C(1s) excitation of carbonate and bicarbonate at the air−water interface. Individual data points indicate the calculated binding energy and the associated coordination number with the anion. Calculated binding energies are "energy-aligned" to the experimental carbonate peak at 289.1 eV. (b) X-ray photoemission C(1s) binding energies with an incident photon energy of 490 eV, from 0.5 M solutions of $NaHCO_3$ and Na_2CO_3. Data in the bottom panel are reproduced from ref 25, copyright 2017, AIP Publishing.

An essential consideration in XPS is the local environment of the excited atom, which has a significant effect on the measured binding energy. Given the different solvation environments between the bulk and surface, one might expect surface effects to modulate the spectra, viz., binding energy shifts or transition narrowing/broadening. These shifts could influence the spectral fitting and, thereby, the relative concentrations of carbonate/bicarbonate reported by Lam et al.

https://doi.org/10.1021/jacs.3c05093
J. Am. Chem. Soc. XXXX, XXX, XXX−XXX

Leveraging the key advantage of real-space KS-DFT for large-scale computations,[54] as well as the recently developed XPS module,[66] we calculate the C K-edge binding energy shifts for carbonate and bicarbonate at the air−water interface, shown in Figure 4a. Our calculations reveal that the XPS spectra were invariant to the displacement of the anion relative to the air−water interface as well as to the coordination number of the carbonate species. In Figure 4b the AP-XPS spectra from Lam et al. are reproduced. The relative shift between the experimental carbonate/bicarbonate spectral signatures agrees well with the shift in the calculated binding energies, with a difference of only ∼0.1 eV, indicating indeed that the spectral fitting and relative concentrations reported by Lam are of the distinct carbonate/bicarbonate peaks and not some convolution of the two due to spectral shifts. These findings imply that the experimental results are largely dictated by the thermodynamic properties and concentration of carbonate species at the interface.

IMPLICATIONS FOR ATMOSPHERIC, ENVIRONMENTAL, AND BIOLOGICAL SCIENCES

The relative partitioning of the carbonate and bicarbonate ions to the air−water interface is of significant environmental and atmospheric importance, for example, in atmospheric aerosol droplet and ocean-surface chemistry. A key consideration to this subject, which has not been discussed in the present work, is the adsorption and dissolution of atmospheric CO_2 from the gas phase. We have previously addressed the solvation and hydrolysis of the species involved in this process by X-ray absorption spectroscopy,[24,26,27] and molecular simulations have highlighted the importance that the interface plays in the adsorption of a polyoxy anion to liquid surfaces.[67]

The ocean serves as a large sink of CO_2 from the atmosphere, with approximately 30% of all anthropogenic CO_2 emissions being absorbed.[68,69] Following solvation into the liquid, carbon dioxide gas hydrolyzes to form carbonic acid, which can further exchange protons to form bicarbonate and carbonate, which is a pH-dependent process:[70]

$$H_2CO_3(aq) + H_2O \rightarrow HCO_3^-(aq) + H_3O^+(aq)\ (pK_a = 6.4) \quad (6)$$

$$HCO_3^-(aq) + H_2O \rightarrow CO_3^{2-}(aq) + H_3O^+(aq)\ (pK_a = 10.3) \quad (7)$$

Thus, an increase in atmospheric CO_2 could greatly impact marine ecosystems via ocean acidification, as given by eqs 6 and 7,[71,72] and will shift the ratio of carbonate and bicarbonate anions present in ocean waters and at the air−ocean interface.

While the ocean has a large degree of buffering capacity, this effect could be quite drastic inside aerosol droplets, which have a high surface area to volume ratios. We have shown here that carbonate resides at the interface in higher quantity than does bicarbonate and expect this partitioning to play an important role in influencing aerosol chemistry. It has been postulated that reaction kinetics can be enhanced at the surfaces of aerosol droplets;[73,74] hence, the change in pH inside of droplets (and subsequent change in surface composition/structure) could disrupt or potentially further enhance these fast reactions. Furthermore, since mammalian respiration systems are also dependent on the buffering capacity of the carbonate system and help to regulate changes in blood pH, a rigorous understanding of carbonate and bicarbonate affinities for, and reactions at, the air−water interface would further illuminate these important topics.

CONCLUSIONS

In this work, we employed resonantly enhanced DUV-SHG to directly probe the carbonate and bicarbonate anions at the air−water interface. By fitting the concentration dependence with a Langmuir adsorption model, we determined that the doubly charged carbonate anion adsorbs more strongly to the surface than singly charged bicarbonate, seemingly in conflict with widely used models and general expectations. These measurements support our previous study of the carbonate system conducted by AP-XPS. We also describe accelerated MD simulations, which revealed that agglomerate formation of the highly charged CO_3^{2-} with Na^+ counterions is the driving force for its surface propensity and that this same behavior is not found for the singly charged HCO_3^-. We hope that these new results will inspire further experiments and modeling to gain deeper insight into this vitally important chemical system.

ASSOCIATED CONTENT

Supporting Information

The Supporting Information is available free of charge at https://pubs.acs.org/doi/10.1021/jacs.3c05093.

Experimental methods and materials and computational Methods; Supporting Tables S1−S4 and Figures S1−S4; complete AMOEBA force field (PDF)

AUTHOR INFORMATION

Corresponding Authors

Jin Qian − *Chemical Sciences Division, Lawrence Berkeley National Lab, Berkeley, California 94720, United States;* orcid.org/0000-0002-0162-0477; Email: jqian2@lbl.gov

Tod A. Pascal − *ATLAS Materials Science Laboratory, Department of Nano Engineering and Chemical Engineering, University of California, San Diego, La Jolla, California 92023, United States; Materials Science and Engineering, University of California San Diego, La Jolla, California 92023, United States; Sustainable Power and Energy Center, University of California San Diego, La Jolla, California 92023, United States;* orcid.org/0000-0003-2096-1143; Email: tpascal@ucsd.edu

Richard J. Saykally − *Department of Chemistry, University of California, Berkeley, California 94720, United States; Chemical Sciences Division, Lawrence Berkeley National Lab, Berkeley, California 94720, United States;* orcid.org/0000-0001-8942-3656; Email: saykally@berkeley.edu

Authors

Shane W. Devlin − *Department of Chemistry, University of California, Berkeley, California 94720, United States; Chemical Sciences Division, Lawrence Berkeley National Lab, Berkeley, California 94720, United States;* orcid.org/0000-0003-3189-5073

Sasawat Jamnuch − *ATLAS Materials Science Laboratory, Department of Nano Engineering and Chemical Engineering, University of California, San Diego, La Jolla, California 92023, United States*

Qiang Xu − *Chemical Sciences Division, Lawrence Berkeley National Lab, Berkeley, California 94720, United States;* orcid.org/0000-0003-3747-4325

https://doi.org/10.1021/jacs.3c05093
J. Am. Chem. Soc. XXXX, XXX, XXX−XXX

Amanda A. Chen − *ATLAS Materials Science Laboratory, Department of Nano Engineering and Chemical Engineering, University of California, San Diego, La Jolla, California 92023, United States;* orcid.org/0000-0002-7358-222X

Complete contact information is available at: https://pubs.acs.org/10.1021/jacs.3c05093

Author Contributions

S.W.D. and S.J. contributed equally.

Notes

The authors declare no competing financial interest.

Additional supporting information (relating to the LAMMPS simulations) have been deposited in https://github.com/atlas-nano/interfacial_carbonates [DOI: 10.5281/zenodo.8327142].

■ ACKNOWLEDGMENTS

This work was supported by the U.S. Department of Energy (DOE), Office of Basic Energy Sciences (BES), Condensed Phase and Interfacial Molecular Science program, through Grant No. DE-SC0023503. S.W.D. and R.J.S. acknowledges support through the Chemical Sciences Division at the Lawrence Berkeley National Laboratory under contract #CH403503. J.Q. and Q.X. were supported by the Gas Phase Chemical Physics and Atomic, Molecular, and Optical Sciences Programs of the U.S. DOE-BES, Chemical Sciences, Geosciences and Biosciences Division, through Contract No. DE-AC0205CH11231. S.J. acknowledges funding from the UC Office of the President within the Multicampus Research Programs and Initiatives (M21PL3263). This research used resources of the National Energy Research Scientific Computing Center, a U.S. DOE Office of Science User Facility supported by the Office of Science of the U.S. Department of Energy under Contract No. DE-AC02-05CH11231 using NERSC awards BES-ERCAP0020767 and BES-ERCAP0024635.

■ REFERENCES

(1) Jubb, A. M.; Hua, W.; Allen, H. C. Organization of Water and Atmospherically Relevant Ions and Solutes: Vibrational Sum Frequency Spectroscopy at the Vapor/Liquid and Liquid/Solid Interfaces. *Acc. Chem. Res.* **2012**, *45* (1), 110−119.

(2) Prophet, A.; Polley, K.; Van Berkel, G.; Limmer, D.; Wilson, K. Iodide Ozonolysis at the Surface of Aqueous Microdroplets; preprint; *ChemRxiv*, **2023**, DOI: 10.26434/chemrxiv-2023-74vpv (accessed 09−08−2023).

(3) Tarbuck, T. L.; Richmond, G. L. Adsorption and Reaction of CO2 and SO2 at a Water Surface. *J. Am. Chem. Soc.* **2006**, *128* (10), 3256−3267.

(4) Sarhangi, S. M.; Waskasi, M. M.; Hashemianzadeh, S. M.; Matyushov, D. V. Effective Dielectric Constant of Water at the Interface with Charged C60 Fullerenes. *J. Phys. Chem. B* **2019**, *123* (14), 3135−3143.

(5) Fumagalli, L.; Esfandiar, A.; Fabregas, R.; Hu, S.; Ares, P.; Janardanan, A.; Yang, Q.; Radha, B.; Taniguchi, T.; Watanabe, K.; et al. Anomalously Low Dielectric Constant of Confined Water. *Science* **2018**, *360* (6395), 1339−1342.

(6) Cox, S. J.; Geissler, P. L. Dielectric Response of Thin Water Films: A Thermodynamic Perspective. *Chem. Sci.* **2022**, *13* (31), 9102−9111.

(7) Odendahl, N. L.; Geissler, P. L. Local Ice-like Structure at the Liquid Water Surface. *J. Am. Chem. Soc.* **2022**, *144* (25), 11178−11188.

(8) Pezzotti, S.; Galimberti, D. R.; Gaigeot, M.-P. 2D H-Bond Network as the Topmost Skin to the Air−Water Interface. *J. Phys. Chem. Lett.* **2017**, *8* (13), 3133−3141.

(9) Zhang, X.-X.; Li, X.-H.; Chen, M. Role of the Electric Double Layer in the Ice Nucleation of Water Droplets under an Electric Field. *Atmospheric Res.* **2016**, *178*, 150−154.

(10) Ong, S.; Zhao, X.; Eisenthal, K. B. Polarization of Water Molecules at a Charged Interface: Second Harmonic Studies of the Silica/Water Interface. *Chem. Phys. Lett.* **1992**, *191* (3−4), 327−335.

(11) Zhao, X.; Ong, S.; Eisenthal, K. B. Polarization of Water Molecules at a Charged Interface. Second Harmonic Studies of Charged Monolayers at the Air/Water Interface. *Chem. Phys. Lett.* **1993**, *202* (6), 513−520.

(12) Hao, H.; Leven, I.; Head-Gordon, T. Can Electric Fields Drive Chemistry for an Aqueous Microdroplet? *Nat. Commun.* **2022**, *13* (1), 1−8.

(13) Jungwirth, P.; Tobias, D. J. Molecular Structure of Salt Solutions: A New View of the Interface with Implications for Heterogeneous Atmospheric Chemistry. *J. Phys. Chem. B* **2001**, *105*, 10468.

(14) Onsager, L.; Samaras, N. N. T. The Surface Tension of Debye-Hückel Electrolytes. *J. Chem. Phys.* **1934**, *2* (8), 528−536.

(15) McCaffrey, D. L.; Nguyen, S. C.; Cox, S. J.; Weller, H.; Alivisatos, A. P.; Geissler, P. L.; Saykally, R. J. Mechanism of Ion Adsorption to Aqueous Interfaces: Graphene/Water vs. Air/Water. *Proc. Natl. Acad. Sci. U. S. A.* **2017**, *114* (51), 13369−13373.

(16) Otten, D. E.; Shaffer, P. R.; Geissler, P. L.; Saykally, R. J. Elucidating the Mechanism of Selective Ion Adsorption to the Liquid Water Surface. *Proc. Natl. Acad. Sci. U. S. A.* **2012**, *109* (3), 701−705.

(17) Devlin, S. W.; Benjamin, I.; Saykally, R. J. On the Mechanisms of Ion Adsorption to Aqueous Interfaces: Air-Water vs. Oil-Water. *Proc. Natl. Acad. Sci. U. S. A.* **2022**, *119* (42), No. e2210857119.

(18) Cameron, F. K.; Seidell, A. Solubility of Calcium Carbonate in Aqueous Solutions of Certain Electrolytes in Equilibrium with Atmospheric Air. *J. Phys. Chem.* **1902**, *6* (1), 50−56.

(19) Yadav, S.; Chandra, A. Structural and Dynamical Nature of Hydration Shells of the Carbonate Ion in Water: An Ab Initio Molecular Dynamics Study. *J. Phys. Chem. B* **2018**, *122* (4), 1495−1504.

(20) Kumar, P. P.; Kalinichev, A. G.; Kirkpatrick, R. J. Hydrogen-Bonding Structure and Dynamics of Aqueous Carbonate Species from Car- Parrinello Molecular Dynamics Simulations. *J. Phys. Chem. B* **2009**, *113* (3), 794−802.

(21) Vchirawongkwin, V.; Sato, H.; Sakaki, S. RISM-SCF-SEDD Study on the Symmetry Breaking of Carbonate and Nitrate Anions in Aqueous Solution. *J. Phys. Chem. B* **2010**, *114* (32), 10513−10519.

(22) Tho, N. M.; Ha, T. K. A Theoretical Study of the Formation of Carbonic Acid from the Hydration of Carbon Dioxide: A Case of Active Solvent Catalysis. *J. Am. Chem. Soc.* **1984**, *106* (3), 599−602.

(23) Kumar, P. P.; Kalinichev, A. G.; Kirkpatrick, R. J. Dissociation of Carbonic Acid: Gas Phase Energetics and Mechanism from Ab Initio Metadynamics Simulations. *J. Chem. Phys.* **2007**, *126* (20), 204315.

(24) England, A. H.; Duffin, A. M.; Schwartz, C. P.; Uejio, J. S.; Prendergast, D.; Saykally, R. J. On the Hydration and Hydrolysis of Carbon Dioxide. *Chem. Phys. Lett.* **2011**, *514* (4−6), 187−195.

(25) Lam, R. K.; Smith, J. W.; Rizzuto, A. M.; Karsl\io\uglu, O.; Bluhm, H.; Saykally, R. J. Reversed Interfacial Fractionation of Carbonate and Bicarbonate Evidenced by X-Ray Photoemission Spectroscopy. *J. Chem. Phys.* **2017**, *146* (9), 94703.

(26) Lam, R. K.; England, A. H.; Sheardy, A. T.; Shih, O.; Smith, J. W.; Rizzuto, A. M.; Prendergast, D.; Saykally, R. J. The Hydration Structure of Aqueous Carbonic Acid from X-Ray Absorption Spectroscopy. *Chem. Phys. Lett.* **2014**, *614*, 282−286.

(27) Lam, R. K.; England, A. H.; Smith, J. W.; Rizzuto, A. M.; Shih, O.; Prendergast, D.; Saykally, R. J. The Hydration Structure of Dissolved Carbon Dioxide from X-Ray Absorption Spectroscopy. *Chem. Phys. Lett.* **2015**, *633*, 214−217.

(28) Brown, M. A.; Lee, M.-T.; Kleibert, A.; Ammann, M.; Giorgi, J. B. Ion Spatial Distributions at the Air–and Vacuum–Aqueous K2CO3 Interfaces. *J. Phys. Chem. C* **2015**, *119* (9), 4976−4982.
(29) Hua, W.; Chen, X.; Allen, H. C. Phase-Sensitive Sum Frequency Revealing Accommodation of Bicarbonate Ions, and Charge Separation of Sodium and Carbonate Ions within the Air/Water Interface. *J. Phys. Chem. A* **2011**, *115* (23), 6233−6238.
(30) Ozdemir, O.; Karakashev, S. I.; Nguyen, A. V.; Miller, J. D. Adsorption of Carbonate and Bicarbonate Salts at the Air–Brine Interface. *Int. J. Miner. Process.* **2006**, *81* (3), 149−158.
(31) Du, H.; Liu, J.; Ozdemir, O.; Nguyen, A. V.; Miller, J. D. Molecular Features of the Air/Carbonate Solution Interface. *J. Colloid Interface Sci.* **2008**, *318* (2), 271−277.
(32) Roy, S.; Mondal, J. A. Kosmotropic Electrolyte (Na2CO3, NaF) Perturbs the Air/Water Interface through Anion Hydration Shell without Forming a Well-Defined Electric Double Layer. *J. Phys. Chem. B* **2021**, *125* (16), 3977−3985.
(33) Ahmed, M.; Nihonyanagi, S.; Kundu, A.; Yamaguchi, S.; Tahara, T. Resolving the Controversy over Dipole versus Quadrupole Mechanism of Bend Vibration of Water in Vibrational Sum Frequency Generation Spectra. *J. Phys. Chem. Lett.* **2020**, *11* (21), 9123−9130.
(34) Matsuzaki, K.; Nihonyanagi, S.; Yamaguchi, S.; Nagata, T.; Tahara, T. Quadrupolar Mechanism for Vibrational Sum Frequency Generation at Air/Liquid Interfaces: Theory and Experiment. *J. Chem. Phys.* **2019**, *151* (6), 064701.
(35) Matsumura, F.; Yu, C.-C.; Yu, X.; Chiang, K.-Y.; Seki, T.; Bonn, M.; Nagata, Y. Does the Sum-Frequency Generation Signal of Aromatic C−H Vibrations Reflect Molecular Orientation? *J. Phys. Chem. B* **2023**, *127* (23), 5288−5294.
(36) Boyd, R. W. *Nonlinear Optics*; Academic Press, 2020.
(37) Petersen, P. B.; Saykally, R. J. Confirmation of Enhanced Anion Concentration at the Liquid Water Surface. *Chem. Phys. Lett.* **2004**, *397*, 51.
(38) Raiteri, P.; Gale, J. D. Water Is the Key to Nonclassical Nucleation of Amorphous Calcium Carbonate. *J. Am. Chem. Soc.* **2010**, *132* (49), 17623−17634.
(39) Catti, M.; Pavese, A.; Price, G. D. Thermodynamic Properties of CaCO3 Calcite and Aragonite: A Quasi-Harmonic Calculation. *Phys. Chem. Miner.* **1993**, *19* (7), DOI: 10.1007/BF00203187.
(40) Pavese, A.; Catti, M.; Parker, S. C.; Wall, A. Modelling of the Thermal Dependence of Structural and Elastic Properties of Calcite, $CaCO_3$. *Phys. Chem. Miner.* **1996**, *23* (2), DOI: 10.1007/BF00202303.
(41) Archer, T. D.; Birse, S. E. A.; Dove, M. T.; Redfern, S. A. T.; Gale, J. D.; Cygan, R. T. An Interatomic Potential Model for Carbonates Allowing for Polarization Effects. *Phys. Chem. Miner.* **2003**, *30* (7), 416−424.
(42) De Leeuw, N. H.; Parker, S. C. Surface−Water Interactions in the Dolomite Problem. *Phys. Chem. Chem. Phys.* **2001**, *3* (15), 3217−3221.
(43) Bruneval, F.; Donadio, D.; Parrinello, M. Molecular Dynamics Study of the Solvation of Calcium Carbonate in Water. *J. Phys. Chem. B* **2007**, *111* (42), 12219−12227.
(44) Raiteri, P.; Schuitemaker, A.; Gale, J. D. Ion Pairing and Multiple Ion Binding in Calcium Carbonate Solutions Based on a Polarizable AMOEBA Force Field and Ab Initio Molecular Dynamics. *J. Phys. Chem. B* **2020**, *124* (17), 3568−3582.
(45) Huang, Y.; Rao, A.; Huang, S.; Chang, C.; Drechsler, M.; Knaus, J.; Chan, J. C. C.; Raiteri, P.; Gale, J. D.; Gebauer, D. Uncovering the Role of Bicarbonate in Calcium Carbonate Formation at Near-Neutral PH. *Angew. Chem., Int. Ed.* **2021**, *60* (30), 16707−16713.
(46) Thompson, A. P.; Aktulga, H. M.; Berger, R.; Bolintineanu, D. S.; Brown, W. M.; Crozier, P. S.; 'T Veld, P. J.; Kohlmeyer, A.; Moore, S. G.; Nguyen, T. D.; Shan, R.; Stevens, M. J.; Tranchida, J.; Trott, C.; Plimpton, S. J. LAMMPS - a Flexible Simulation Tool for Particle-Based Materials Modeling at the Atomic, Meso, and Continuum Scales. *Comput. Phys. Commun.* **2022**, *271*, 108171.
(47) Ponder, J. W.; Wu, C.; Ren, P.; Pande, V. S.; Chodera, J. D.; Schnieders, M. J.; Haque, I.; Mobley, D. L.; Lambrecht, D. S.; DiStasio, R. A.; Head-Gordon, M.; Clark, G. N. I.; Johnson, M. E.; Head-Gordon, T. Current Status of the AMOEBA Polarizable Force Field. *J. Phys. Chem. B* **2010**, *114* (8), 2549−2564.
(48) Byrne, E. H.; Raiteri, P.; Gale, J. D. Computational Insight into Calcium−Sulfate Ion Pair Formation. *J. Phys. Chem. C* **2017**, *121* (46), 25956−25966.
(49) Barducci, A.; Bussi, G.; Parrinello, M. Well-Tempered Metadynamics: A Smoothly Converging and Tunable Free-Energy Method. *Phys. Rev. Lett.* **2008**, *100* (2), 020603.
(50) Bussi, G.; Laio, A.; Parrinello, M. Equilibrium Free Energies from Nonequilibrium Metadynamics. *Phys. Rev. Lett.* **2006**, *96* (9), 090601.
(51) Ensing, B.; De Vivo, M.; Liu, Z.; Moore, P.; Klein, M. L. Metadynamics as a Tool for Exploring Free Energy Landscapes of Chemical Reactions. *Acc. Chem. Res.* **2006**, *39* (2), 73−81.
(52) Raiteri, P.; Laio, A.; Gervasio, F. L.; Micheletti, C.; Parrinello, M. Efficient Reconstruction of Complex Free Energy Landscapes by Multiple Walkers Metadynamics. *J. Phys. Chem. B* **2006**, *110* (8), 3533−3539.
(53) Fiorin, G.; Klein, M. L.; Hénin, J. Using Collective Variables to Drive Molecular Dynamics Simulations. *Mol. Phys.* **2013**, *111* (22−23), 3345−3362.
(54) Xu, Q.; Wang, S.; Xue, L.; Shao, X.; Gao, P.; Lv, J.; Wang, Y.; Ma, Y. Ab Initio Electronic Structure Calculations Using a Real-Space Chebyshev-Filtered Subspace Iteration Method. *J. Phys.: Condens. Matter* **2019**, *31* (45), 455901.
(55) Kameda, Y.; Sasaki, M.; Hino, S.; Amo, Y.; Usuki, T. Neutron Diffraction Study on the Hydration Structure of Carbonate Ion by Means of 12C/13C Isotopic Substitution Method. *Phys. B Condens. Matter* **2006**, *385*, 279−281.
(56) Rudolph, W. W.; Fischer, D.; Irmer, G. Vibrational Spectroscopic Studies and Density Functional Theory Calculations of Speciation in the CO2—Water System. *Appl. Spectrosc.* **2006**, *60* (2), 130−144.
(57) Devlin, S. W.; McCaffrey, D. L.; Saykally, R. J. Characterizing Anion Adsorption to Aqueous Interfaces: Toluene–Water versus Air–Water. *J. Phys. Chem. Lett.* **2022**, *13*, 222−228.
(58) Petersen, P. B.; Johnson, J. C.; Knutsen, K. P.; Saykally, R. J. Direct Experimental Validation of the Jones–Ray Effect. *Chem. Phys. Lett.* **2004**, *397* (1−3), 46−50.
(59) Petersen, P. B.; Saykally, R. J. *Probing the Interfacial Structure of Aqueous Electrolytes with Femtosecond Second Harmonic Generation Spectroscopy*; ACS Publications, 2006.
(60) Okur, H. I.; Chen, Y.; Wilkins, D. M.; Roke, S. The Jones-Ray Effect Reinterpreted: Surface Tension Minima of Low Ionic Strength Electrolyte Solutions Are Caused by Electric Field Induced Water-Water Correlations. *Chem. Phys. Lett.* **2017**, *684*, 433−442.
(61) Chen, Y.; Okur, H. I.; Gomopoulos, N.; Macias-Romero, C.; Cremer, P. S.; Petersen, P. B.; Tocci, G.; Wilkins, D. M.; Liang, C.; Ceriotti, M. Electrolytes Induce Long-Range Orientational Order and Free Energy Changes in the H-Bond Network of Bulk Water. *Sci. Adv.* **2016**, *2* (4), No. e1501891.
(62) Bian, H.; Feng, R.; Xu, Y.; Guo, Y.; Wang, H. Increased Interfacial Thickness of the NaF, NaCl and NaBr Salt Aqueous Solutions Probed with Non-Resonant Surface Second Harmonic Generation (SHG). *Phys. Chem. Chem. Phys.* **2008**, *10* (32), 4920−4931.
(63) Marcus, Y. Thermodynamics of Solvation of Ions. Part 5.—Gibbs Free Energy of Hydration at 298.15 K. *J. Chem. Soc. Faraday Trans.* **1991**, *87* (18), 2995−2999.
(64) Jungwirth, P.; Tobias, D. J. Specific Ion Effects at the Air/Water Interface. *Chem. Rev.* **2006**, *106* (4), 1259−1281.
(65) Jubb, A. M.; Hua, W.; Allen, H. C. Environmental Chemistry at Vapor/Water Interfaces: Insights from Vibrational Sum Frequency Generation Spectroscopy. *Annu. Rev. Phys. Chem.* **2012**, *63* (1), 107−130.

https://doi.org/10.1021/jacs.3c05093
J. Am. Chem. Soc. XXXX, XXX, XXX−XXX

(66) Xu, Q.; Prendergast, D.; Qian, J. Real-Space Pseudopotential Method for the Calculation of 1 *s* Core-Level Binding Energies. *J. Chem. Theory Comput.* **2022**, *18* (9), 5471−5478.
(67) Galib, M.; Limmer, D. T. Reactive Uptake of N2O5 by Atmospheric Aerosol Is Dominated by Interfacial Processes. *Science* **2021**, *371* (6532), 921−925.
(68) Sabine, C. L.; Feely, R. A.; Gruber, N.; Key, R. M.; Lee, K.; Bullister, J. L.; Wanninkhof, R.; Wong, C. S. L.; Wallace, D. W. R.; Tilbrook, B.; et al. The Oceanic Sink for Anthropogenic CO2. *science* **2004**, *305* (5682), 367−371.
(69) Gruber, N.; Clement, D.; Carter, B. R.; Feely, R. A.; Van Heuven, S.; Hoppema, M.; Ishii, M.; Key, R. M.; Kozyr, A.; Lauvset, S. K.; et al. The Oceanic Sink for Anthropogenic CO2 from 1994 to 2007. *Science* **2019**, *363* (6432), 1193−1199.
(70) Langmuir, D. *Aqueous Environmental Geochemistry*; Prentice Hall: Upper Saddle River, NJ, 1997; p 600.
(71) Hoegh-Guldberg, O.; Poloczanska, E. S.; Skirving, W.; Dove, S. Coral Reef Ecosystems under Climate Change and Ocean Acidification. *Front. Mar. Sci.* **2017**, *4*, 158.
(72) Cao, L.; Caldeira, K.; Jain, A. K. Effects of Carbon Dioxide and Climate Change on Ocean Acidification and Carbonate Mineral Saturation. *Geophys. Res. Lett.* **2007**, *34* (5), DOI: 10.1029/2006GL028605.
(73) Lee, J. K.; Kim, S.; Nam, H. G.; Zare, R. N. Microdroplet Fusion Mass Spectrometry for Fast Reaction Kinetics. *Proc. Natl. Acad. Sci. U. S. A.* **2015**, *112* (13), 3898−3903.
(74) Lee, J. K.; Banerjee, S.; Nam, H. G.; Zare, R. N. Acceleration of Reaction in Charged Microdroplets. *Q. Rev. Biophys.* **2015**, *48* (4), 437−444.

https://doi.org/10.1021/jacs.3c05093
J. Am. Chem. Soc. XXXX, XXX, XXX−XXX